Carbohydrate Polymers 96 (2013) 611–620

Contents lists available at SciVerse ScienceDirect

Carbohydrate Polymers

journal homepage: www.elsevier.com/locate/carbpol

Poly(lactic acid)/natural rubber/cellulose nanocrystal bionanocomposites Part I. Processing and morphology

Natacha Bitinis[a], Raquel Verdejo[a], Julien Bras[b], Elena Fortunati[c], Jose Maria Kenny[a,c], Luigi Torre[c], Miguel Angel López-Manchado[a,*]

[a] Institute of Polymer Science and Technology, ICTP-CSIC, C/Juan de la Cierva 3, 28006 Madrid, Spain
[b] Lab Pulp & Paper Science, LGP2, F-38402 St Martin Dheres, France
[c] University of Perugia, UdR INSTM, Department of Civil & Environmental Engineering, I-05100 Terni, Italy

ARTICLE INFO

Article history:
Received 15 December 2012
Received in revised form 21 January 2013
Accepted 21 February 2013
Available online 6 March 2013

Keywords:
Cellulose nanocrystal
Surface modification
Bionanocomposite
Poly(lactic acid)
Melt blending
Morphology

ABSTRACT

PLA/NR/cellulose nanowhisker composites were prepared using three types of cellulose nanocrystals (CNC), i.e. unmodified CNC obtained from acid hydrolysis of microcrystalline cellulose and two surface modified CNC. The two modification reactions, consisting on the grafting of long alkyl chains and of PLA chains onto the cellulose nanocrystals were carried out in order to facilitate the incorporation of the nanocrystals in the PLA/NR blend. A novel processing method was optimized combining solvent casting and extrusion in order to obtain a homogeneous dispersion of the nanofillers in the blend. The CNC modifications determined their location in the PLA/NR blend and influenced its morphology.

1. Introduction

In recent years, the development of bionanocomposites has attracted both industrial and academic attention due to the increasing interest on developing new sustainable and environmentally friendly materials. Bionanocomposites can be considered as a subset of polymer nanocomposites where the nanofillers, the matrix or both come from bio-based, renewable resources. Moreover, adding nanofillers into biopolymers presents a practical way to improve the properties of these bioplastics, making them competitive with petroleum-derived materials (Bordes, Pollet, & Averous, 2009; Darder, Aranda, & Ruiz-Hitzky, 2007; Rhim, 2007). Especially, bionanoparticles such as cellulose or starch nanowhiskers present the advantage of being renewable when compared to other inorganic nanofillers such as layered silicates (Habibi, Lucia, & Rojas, 2010; Le Corre, Bras, & Dufresne, 2010). High strength cellulose nanocrystals (CNC) can be obtained from acid hydrolysis of cellulose fibers and are typically rod-like particles with a diameter of few nanometers and a length varying from tens to hundreds nanometers (Bondeson & Oksman, 2007). The first study of reinforced polymer matrix using this new type of nanofillers reported excellent mechanical properties, motivating academic research (Favier et al., 1995). Particular interest has been drawn to the reinforcement of poly(lactic acid) (PLA), which is one of the most promising biopolymers for a wide range of industrial applications (Fortunati et al., 2012b; Pei, Zhou, & Berglund, 2010; Petersson, Kvien, & Oksman, 2007).

On another hand, it has been demonstrated that nanoparticles could behave as effective compatibilizers for immiscible polymer blends through their preferential location at the polymer interfaces, reducing the interfacial tension and preventing the coalescence of the dispersed phase (Fenouillot, Cassagnau, & Majeste, 2009). In our previous reports, we demonstrated the compatibilizing effect of different organoclays on an immiscible poly(lactic acid)/natural rubber blend (PLA/NR 90/10 wt.%), resulting in a decrease of the NR droplet size from 1 μm up to 300 nm. Moreover, interesting properties were obtained for these nanocomposites, which could be optimized depending on their surface properties (Bitinis et al., 2012a, 2012b). Nevertheless, it would be of interest to substitute these inorganic nanofillers by bionanoparticles in our bio-based blend and to observe for the first time their behavior in immiscible polymer blends.

Cellulose nanowhiskers present several drawbacks for the preparation of polymer nanocomposites by melt blending when compared to organoclays. Firstly, their incorporation into polymeric matrix has initially been limited to hydrosoluble polymers

* Corresponding author. Tel.: +34 915 622 900; fax: +34 915 644 853.
E-mail address: lmanchado@ictp.csic.es (M.A. López-Manchado).

0144-8617/$ – see front matter © 2013 Elsevier Ltd. All rights reserved.
http://dx.doi.org/10.1016/j.carbpol.2013.02.068

or to emulsion polymers due to their hydrophilic characteristics (Angellier, Molina-Boisseau, Lebrun, & Dufresne, 2005; Favier et al., 1995) and surface modifications are often required to improve their compatibility with the polymer matrices. Another drawback of these bionanoparticles is their strong aggregation when drying. Cellulose nanowhiskers form a thin film while microfibrillated cellulose forms an extremely tough nanopaper, due to strong hydrogen bonds (Henriksson, Berglund, Isaksson, Lindstrom, & Nishino, 2008). Freeze-drying is the best option to dry cellulose nanowhiskers but redispersion in polymeric matrices remains a major issue. Moreover, bionanoparticles present a low thermal stability and could be subjected to degradation during melt mixing (Goffin et al., 2011a).

Based on this information and given our results for PLA/NR/organoclays nanocomposites, we report in this work the preparation of PLA/NR/CNC bionanocomposites. CNC were extracted by acid hydrolysis of microcrystalline cellulose and two modification reactions were planned. One functionalization involved the grafting of long alkyl chains on the CNC surface following the chemical modification proposed by Siqueira, Bras, and Dufresne (2010). Such modification was pursued due to the interesting mechanical properties of our nanocomposite blend prepared with montmorillonite modified with cations possessing two alkyl tallows (C15A). Additionally, the layered silicate nanocomposite study showed that obtaining a reinforced PLA matrix while maintaining the large deformation under tensile conditions obtained for the PLA/NR blend remained an issue. Thus, the preparation of a nanohybrid consisting of CNC grafted with short chains of PLA was deemed as a possible solution as such chains could preserve the material ductility. Such nanohybrids were prepared by ring opening polymerization. Thus, here we describe the properties of the cellulose nanocrystals, with a special attention toward its thermal degradation, as well as the preparation of the bionanocomposites, their morphology and rheological properties.

2. Experimental

2.1. Materials

Microcrystalline cellulose (MCC), sulfuric acid (96%), *n*-octadecyl isocyanate, dibutyltin dilaurate, L-lactide, Tin (II) 2-ethylhexanoate, chloroform, dichloromethane anhydrous and toluene anhydrous, were provided by Sigma–Aldrich. Acetone and ethanol were purchased from Chimie-Plus.

PLA polymer 2002D was provided by NatureWorks® (D-content 4.25%, MI = 5–7 g/10 min, $\rho = 1.24\ g\ cm^{-3}$). Natural Rubber (NR) was kindly supplied by Malaysian Rubber under the trade name CV60 (Mooney viscosity: ML(1 + 4) 100 °C = 60, $\rho = 0.91\ g\ cm^{-3}$).

2.2. Synthesis and functionalization of the cellulose nanocrystals

Cellulose nanocrystals (CNC) were produced from sulfuric acid treatment of microcrystalline cellulose (MCC) following the procedure of Bondeson, Mathew, and Oksman (2006). Repeated centrifugation cycles (Sigma laboratory centrifuges 6K15, 10,000 rpm, 10 min, 4 °C) with deionized water were then carried out to wash the obtained suspension (at least five washings). Finally, the suspension was dialyzed against deionized water for about 5 days until the wash water reached a constant pH and the recovered CNC suspension was neutralized using a 1 wt.% NaOH solution. The aqueous suspension was kept at 4 °C after adding a few drops of chloroform as an anti-bacterial agent. The yield reaction was about 20%.

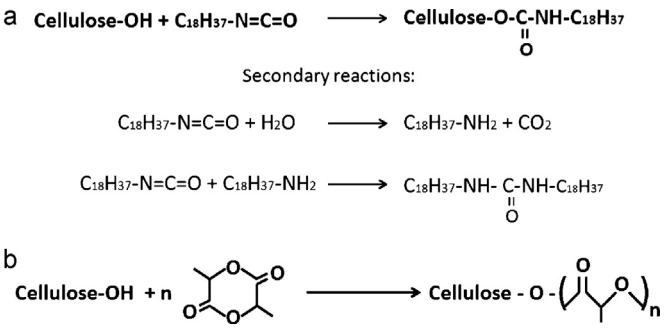

Fig. 1. Surface grafting reaction of (a) *n*-octadecyl isocyanate with the hydroxyl group on the CNC surface and secondary reactions, (b) PLA chains by ring opening polymerization.

The CNC surface grafting with *n*-octadecyl isocyanate was carried out following the procedure developed by Siqueira et al. (2010) (Fig. 1a). The aqueous suspension containing CNC was solvent-exchange by successive centrifugation steps from deionized water to acetone, and from acetone to anhydrous toluene, solvent in which the grafting reaction took place. This process avoids drying the CNC, which would lead to strong aggregation of the crystals reducing the available surface for the reaction. Afterward, a centrifugation protocol consisting in several cycles with different solvents (1 cycle of toluene, 4 cycles of dichloromethane and 3 cycles of ethanol) was performed to remove the secondary products and the un-reacted isocyanate. Modified CNC with long carbon chains is denoted as C18-g-CNC.

The CNC surface grafting with PLA chains by in situ ring opening polymerization of L-lactide was adapted from Goffin et al. (2011a) (Fig. 1b). Again, the aqueous suspension containing the CNC was solvent-exchange by successive centrifugation steps from deionized water to acetone, and from acetone to anhydrous toluene. After the 24 h reaction, the secondary products, un-reacted L-lactide and the non-grafted polymer were removed using a centrifugation protocol, established after having testing several possibilities (4 cycles of methanol, 4 cycles of ethanol and 2 cycles of acetone). The advantage of this procedure when compared to a Soxhlet extraction is that a lower amount of nanofillers is lost through the Soxhlet cartridge. Modified CNC with PLA chains is denoted as PLA-g-CNC.

2.3. Processing of the bionanocomposites

Two methods were used to prepare the nanocomposites, i.e. direct extrusion or solvent casting combined with extrusion (Haake Minilab twin screw extruder). For direct extrusion, CNC were lyophilized for 48 h (lyophilizator Telstar Lioalfa-6), forming a foam that was then pulverized in an analytical grinder from IKA. Through direct extrusion, the obtained powder was mixed with PLA/NR blend in the extruder (160 °C, 100 rpm, 15 min). PLA were dried overnight at 80 °C in a ventilated oven prior to use. NR concentration in the blend was fixed at 10 wt.% and both PLA and NR were dried mixed before melt blended in the extruder due to the difficulty of introducing NR into the extruder. Once a homogeneous blend is obtained, CNC is added into the extruder. For solvent casting combined with extrusion, a pre-blend of PLA/CNC was first prepared. For this purpose, CNC were solvent exchange from water to acetone and from acetone to chloroform by several centrifugation cycles. The suspension was sonicated for 3×3 min with an ultrasonication probe (Sonics Vibracell) in an ice bath to avoid temperature rise and was added to a PLA solution in $CHCl_3$ previously prepared. PLA/CNC mixture was then stirred for 1 h and sonicated for 15 min using on/off cycles in order to avoid overheating. PLA/CNC mixture was then casted and $CHCl_3$ was allowed to evaporate for 2 days at room temperature, 5 h under vacuum

at 40 °C and dried over night before used in a ventilated oven at 80 °C. PLA/CNC film was cut into small pieces and dried mixed with NR before being extruded (160 °C, 100 rpm, 15 min). For the sake of comparison, the unfilled PLA/NR blend was prepared following the same protocol as CNC filled samples, i.e. PLA was dissolved in $CHCl_3$, casted and dried under the exact same conditions as for the PLA/CNC mixture, the PLA film being then cut and extruded with NR.

NR concentration was fixed at 10 wt.% and the cellulose nanocrystal loading was varied from 1 to 5 wt.%. Samples prepared by direct extrusion were coded as _E (for example PLA/NR/CNC_E) while no specific indication in nomenclature was made for the samples prepared by combining solvent casting and extrusion.

2.4. Characterizations

2.4.1. Cellulose nanocrystals

An environmental scanning electron microscope (ESEM), model Quanta 200 FEI, with accelerating voltage of 10 kV was used to characterize the MCC.

TEM images of unmodified and modified cellulose nanowhiskers were obtained in a LEO 910 microscope with a bioscan camera model 792. The samples were prepared by drop-casting a previously sonicated diluted suspension of CNC in water (in order to avoid the damage of the carbon grid) and allowing the water to evaporate. The samples were stained with a 2 wt.% uranyl acetate solution for about 5 min.

X-ray diffraction (XRD) was used to evaluate the crystallinity of the cellulose nanowhiskers. The experiments were performed in a D8 Advance equipment from Bruker with a CuKα radiation at λ = 1.54 Å (40 kV and 40 mA). Measurements were carried out in a range from 1° to 30° of 2θ at 0.2 s per point.

Fourier transform infrared spectra (FT-IR) were obtained on a Perkin-Elmer Spectrum One with a resolution of 4 cm^{-1}. FT-IR spectra were recorded by depositing the cellulose powder directly on the surface crystals with the ATR configuration.

Elemental analysis of the sample was carried out in a Leco CHNS-932 apparatus in order to determine the weight percentage of carbon, hydrogen, nitrogen, and sulfur present in the sample. The experiments were performed by heating about 2 mg of sample to 1000 °C. The amounts of C, H and S were measured by an IR absorption detection system and the percentage of nitrogen by a thermal conductivity detector.

Thermogravimetric analysis-mass spectrometry (TGA-MS) measurements were performed using a Mettler Toledo thermogravimetric analyzer (TGA, model TA Q500) coupled to a Pfeiffer Vacuum ThermoStar TM mass spectrometer, in order to analyze the products resulting from the decomposition of the sample. The temperature program was run from 30 °C to 900 °C at a heating rate of 5 °C min^{-1} in helium atmosphere (20 ml min^{-1}).

2.5. Bionanocomposites

Rheological measurements were performed using an ARES Advanced Rheometric Expansion System rheometer with parallel plate geometry of 25 mm of diameter. Tests were carried out in dynamic mode of shearing at 180 °C from 0.01 rad s^{-1} to 100 rad s^{-1} frequency range.

The morphology of the samples was observed using a Philips XL30 environmental scanning electron microscopy (ESEM) at 15 kV. All the samples were cryo-fractured in liquid nitrogen and the fracture surface was sputter coated with gold/palladium (Au/Pd 80/20). The nanowhisker dispersion was also studied by transmission electron microscopy (Philips Tecnai 20 microscope at an acceleration voltage of 200 kV). Ultra-thin sections of the samples were prepared by cryo-ultramicrotomy at −140 °C (Leica EM UC6). The rubber droplet size was determined by image analysis using ImageJ (Rasband, W. 1997–2009, ImageJ software, http://rsb.info.nih.gov/ij/. ImageJ, US, Bethesda, Maryland, USA: National Institutes of Health). Typically, 200 droplets were analyzed per sample and the average Feret's diameter was calculated.

3. Results and discussion

3.1. Characterization of cellulose nanocrystals

3.1.1. Unmodified cellulose nanocrystals

The acid hydrolysis of MCC leads to the removal of the amorphous cellulose and to the production of rod-like nanocrystals, as shown in Fig. 2a. Individual cellulose whiskers obtained from water suspension can be observed. The stability of CNC colloidal suspension in water depends on the dimension and polydispersity of the crystals, but also on their surface charges, due to the presence of sulfate groups remaining from the hydrolysis (Azizi Samir, Alloin, & Dufresne, 2005; Beck-Candanedo, Roman, & Gray, 2005). The average length of cellulose nanowhiskers determined by image analysis (ImageJ software, 200 measurements) was 250 ± 80 nm (Fig. 2a). The value of the diameter is reported in the literature to be between 5 and 10 nm, and is in agreement with the images (Bondeson et al., 2006; Habibi et al., 2010).

The study of the thermal degradation of CNC is of major importance, especially regarding the melt processing of the nanocomposites. Here, it was analyzed by thermogravimetric analysis coupled with mass spectrometry (Fig. 3a). The initial weight loss up to 230 °C of approximately 10% can be ascribed to the presence of absorbed water. Then, the degradation occurs in a broad temperature range, being separated in two defined processes. The first one occurs between 230 °C and 300 °C while the second one is a high temperature (from 350 °C to 650 °C) and slow process, resulting in a large amount of residues. This behavior has been observed by other authors and attributed to the presence of sulfate groups remaining from the acid hydrolysis (Fortunati et al., 2012a; Wang, Ding, & Cheng, 2007)

The effect of acid washing over the cellulose pyrolysis has been reported years ago, by studying the possible flame retardancy effect of sulfuric acid in the pyrolysis and combustion of cellulose (Julien, Chornet, & Overend, 1993; Kim, Nishiyama, Wada, & Kuga, 2001; Pappa, Mikedi, Tzamtzis, & Statheropoulos, 2006; Pappa, Tzamtzis, Statheropoulos, Liodakis, & Parissakis, 1995; Statheropoulos & Kyriakou, 2000). The authors explained that the presence of inorganic acids increased the yield char at the expense of flammable tars but lower the onset of the thermal degradation. In fact, sulfuric acid can react with the cellulose hydroxyl groups to form sulfate ester. As the temperature increases, the ester decomposes forming an organic sulfate and leading to the dehydration of the cellulose, facilitated by the low energy required to eliminate the sulfate acid in the sulfated anhydroglucose units. Thus, sulfuric acid could be considered as a dehydration catalyst. Moreover, decompositions involving the dehydration reaction increase the formation of gas, char, acid and carbonyl compounds, such as hydroxyacetaldehyde. This dehydration mechanism occurs at the expense of other degradation mechanisms, such as depolymerization. The depolymerization mechanisms lead to the formation of levoglucosan and other volatile products. These observations corresponded to cellulose impregnated with acid solution and the authors analyzed the char residue by FT-IR or the gaseous products of pyrolysis by mass spectrometry (Julien et al., 1993; Pappa et al., 1995, 2006).

Thus, the sulfuric acid hydrolysis for the preparation of the cellulose nanowhiskers is expected to have a strong influence over the degradation of the cellulose. Roman and Winter (2004) studied the effect of hydrolysis conditions on the thermal degradation behavior

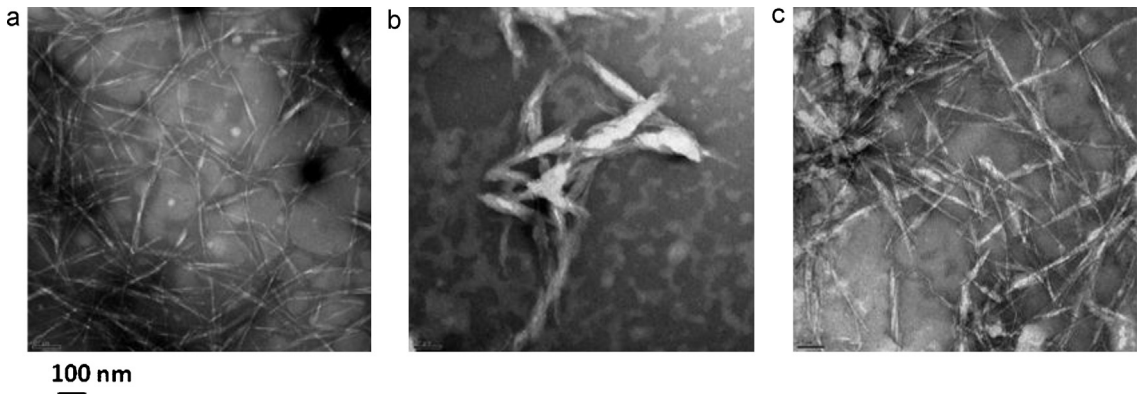

Fig. 2. TEM images of (a) CNC, (b) C18-g-CNC and (c) PLA-g-CNC.

of bacterial cellulose. They demonstrated that the introduction of sulfate groups at the crystal surface during acid hydrolysis caused a significant decrease of the degradation temperature. Two processes were identified, the first one being attributed to the degradation of more accessible, highly sulfated regions while the second one was related to the breakdown of the unsulfated crystal interior. Similarly, Wang et al. (2007) studied the hydrolysis conditions of MCC and neutralization procedures of the CNC. The nanowhiskers with detectable sulfate acid groups presented the two-steps process, as the result of a primary pyrolysis catalyzed by acid sulfate groups and of a low charring process of the solid residue.

Here, the identification of the degradation process is carried out by thermogravimetric analysis coupled to mass spectrometry. Signals for $m/z = 48$ and $m/z = 64$ are detected at about 280 °C during the first degradation step of CNC and can be attributed to sulfate species (Pappa et al., 1995). At higher temperature, between 300 and 400 °C, carbon dioxide and monoxide are detected ($m/z = 25$ and 44), as well as masses related to anhydro sugars such as levoglucosan ($m/z = 43$, 57, 60, 70, 73 and 144) and levoglucosenone ($m/z = 39$, 42, 52, 53, 96) (Pappa, Mikedi, Tzamtzis, & Statheropoulos, 2003). Mass at $m/z = 60$ could also be related to acetic acid and hydroxyacetaldehyde (Franklin, 1979). A slow degradation process is observed at temperatures higher than 400 °C, as well as a gradual increase of the signal intensity for $m/z = 44$, corresponding to CO_2. This process is then attributed to the charring process of the solid residue.

3.1.2. Characterization of the grafting reactions

The proposed surface modification reactions of the CNC are represented in Fig. 1. The grafting of long alkyl chains onto the nanocrystal surface results from the reaction of *n*-octadecyl isocyanate with the hydroxyl groups of cellulose. However, isocyanate

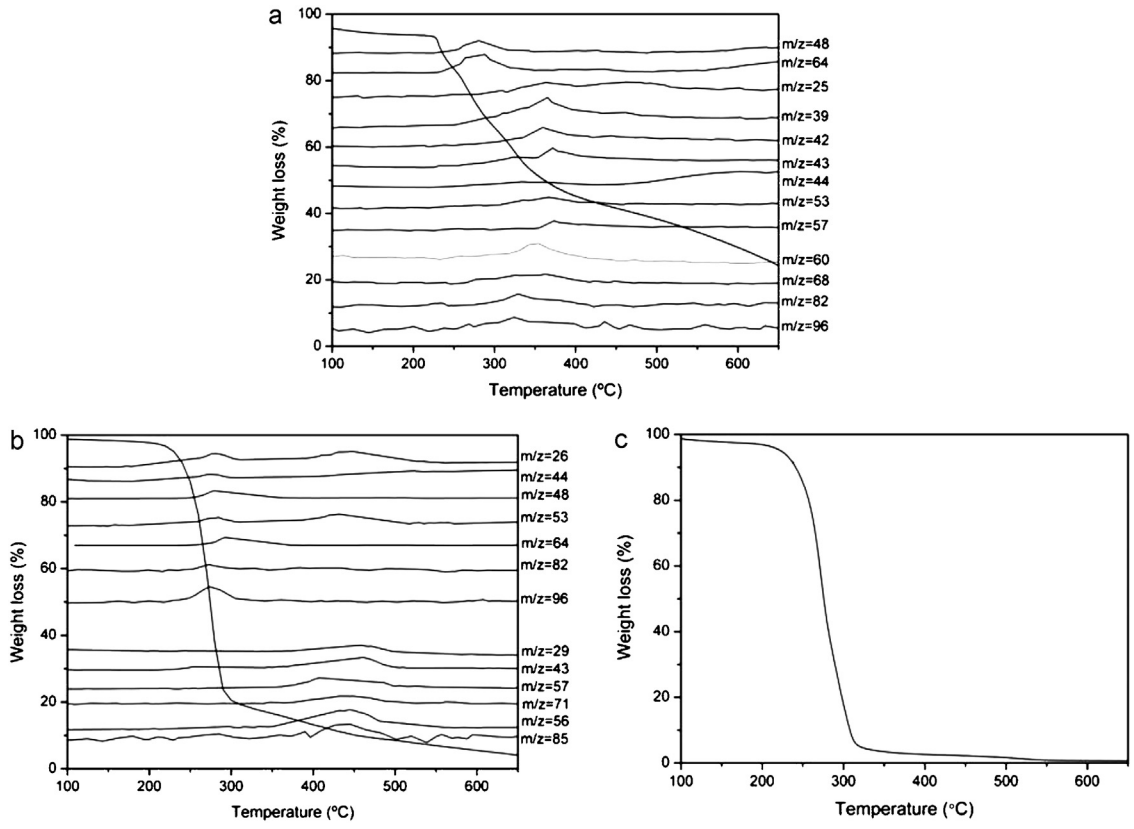

Fig. 3. TGA analysis coupled with mass spectrometry of (a) CNC, (b) C18-g-CNC and (c) TGA analysis of PLA-g-CNC.

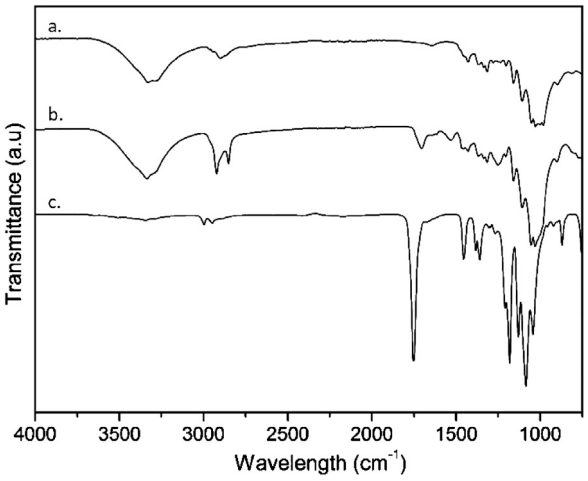

Fig. 4. FT-IR of (a) CNC, (b) C18-g-CNC and (c) PLA-g-CNC.

groups are highly reactive with water resulting in the formation of disubstituted urea and carbon dioxide (Fig. 1a). Hence, the reaction was carried out with an excess of isocyanate to counterbalance this possibility. Meanwhile, PLA grafting onto cellulose nanocrystals occurs by ring opening polymerization (Fig. 1b).

Fig. 4 shows the FT-IR spectra of CNC, C18-g-CNC and PLA-g-CNC. CNC spectrum (Fig. 4a) shows the typical absorption bands of cellulose: —OH group at 3300 cm^{-1}, —C—H and —CH_2— at 2850 and 2900 cm^{-1} and —C—O— at 1030 cm^{-1}.

After the alkyl chain grafting reaction (Fig. 4b), two intense bands at 2920 and 2850 cm^{-1} attributed to the —CH_2— and —CH_3 groups confirm the presence of long alkyl chains. Moreover, the grafting efficiency is demonstrated by the appearance of a new signal at 1704 cm^{-1} associated to the carbamate group formed during the reaction. The removal of the excess of isocyanate is verified by the absence of the isocyanate group signal at 2260 cm^{-1}. The analysis of the by-products also confirms the formation of long chains of diurea, observed as two strong absorption bands at 1610 and 1570 cm^{-1} corresponding to the amide function groups (data not shown). The absence of these two bands in the final product validates the efficiency of the centrifugation cycles as an effective washing method.

PLA-g-CNC presents the typical sharp band at 1750 cm^{-1} of the carbonyl group stretching (—C=O) and the —C—O— stretching band of the —CH—O— group at 1182 cm^{-1} of PLA, as well as the weak band at 3300 cm^{-1} of O—H groups of the cellulose. The absence of L-LA absorption band at 1240 and 1270 cm^{-1} in the FT-IR spectra of the final PLA-g-CNC suggests the effective removal of residual monomer during the centrifugations. Chloroform centrifugation steps were tried as a method to remove residues of non-grafted PLA polymer. However, PLA-g-CNC crystals did not sediment in chloroform even after several centrifugation cycles. This is a clear evidence of the successful grafting of PLA onto CNC surface.

Moreover, the grafting content for both reactions was determined from elemental analysis. The content of the N element in C18-g-CNC ($N_{C18\text{-}g\text{-}CNC}$) was determined to be 1.1%, while the theoretical N element content in the *n*-octadecyl isocyanate (N_{C18}) is 4.7%. Thus, the content *x* of grafted chains could be evaluated with the following equation (Lin, Chen, Huang, Dufresne, & Chang, 2009):

$$xN_{C18} = N_{C18-g-CNC} \quad (1)$$

Hence, a content of 23 wt.% of grafted carbon chains is obtained.

In a similar way, the content of the C element in CNC (C_{CNC}) and PLA-g-CNC ($C_{PLA\text{-}g\text{-}CNC}$) were determined to be 38.6% and 46.7% respectively, while the theoretical C element content in the PLA (C_{PLA}) is 50%. Following the equation:

$$xC_{PLA} + (1-x)C_{CNC} = C_{PLA-g-CNC} \quad (2)$$

a content of 70 wt.% of PLA in PLA-g-CNC is obtained.

A corroboration of these results was carried out by TGA analysis, as shown in Fig. 3b and c. For C18-g-CNC (Fig. 3b), the first strong degradation step is attributed to the degradation of CNC, as *m*/*z* signals previously observed for the unmodified cellulose nanocrystal degradation are detected at 280 °C. This temperature is lower than for unmodified CNC (signals detected between 300 and 350 °C), which indicates a decrease of thermal stability after the grafting reaction. This behavior has been reported by Uschanov, Johansson, Maunu, and Laine (2011) for cellulose modified with long-chain fatty acids by esterification reaction and was attributed to a change of crystallinity in the surface structure, owing to the modification reaction (see structural analysis). Signals at 450 °C are observed for $m/z = 29 + n14$ and can be attributed to the fragmentation and degradation of the grafted carbon chains. Moreover, the signal at $m/z = 56$ could indicate the formation of the CH_2NCO^+ cation. The amount of grafted chains is then also estimated to be around 20%.

Fig. 3c shows the thermal degradation of PLA-g-CNC. Nevertheless, the degradation steps of CNC and PLA appear to overlap and no clear conclusions can be made.

Structural characterization of the cellulose nanowhiskers was carried out by TEM and XRD analysis. Fig. 2b and c shows the TEM images of C18-g-CNC and PLA-g-CNC, respectively. C18-g-CNC are less individualized than unmodified CNC. In fact, C18-g-CNC are less stable in water due to the presence of long hydrophobic carbon chains, resulting in the formation of nanowhisker agglomerates.

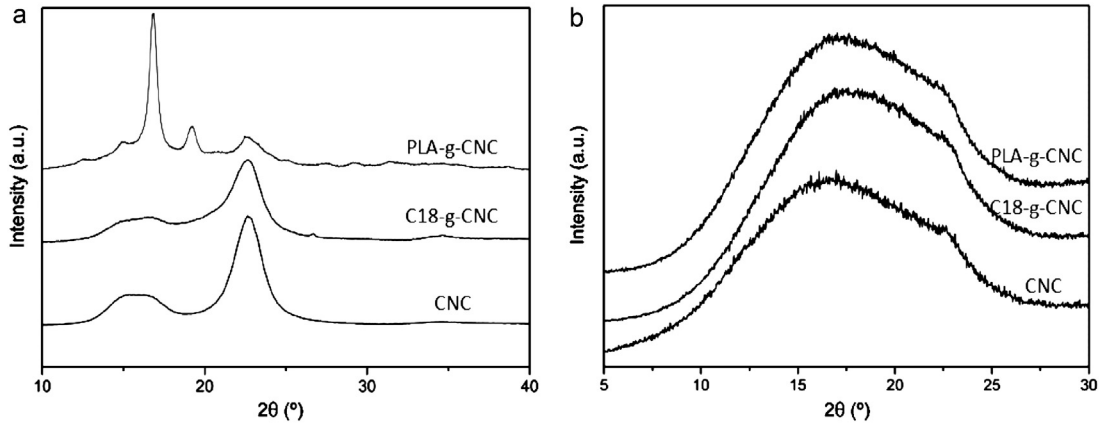

Fig. 5. XRD of (a) cellulose nanocrystals and of (b) PLA/NR/cellulose nanocrystals nanocomposites at 3 wt.% of CNC and 5 wt.% of C18-g-CNC and PLA-g-CNC.

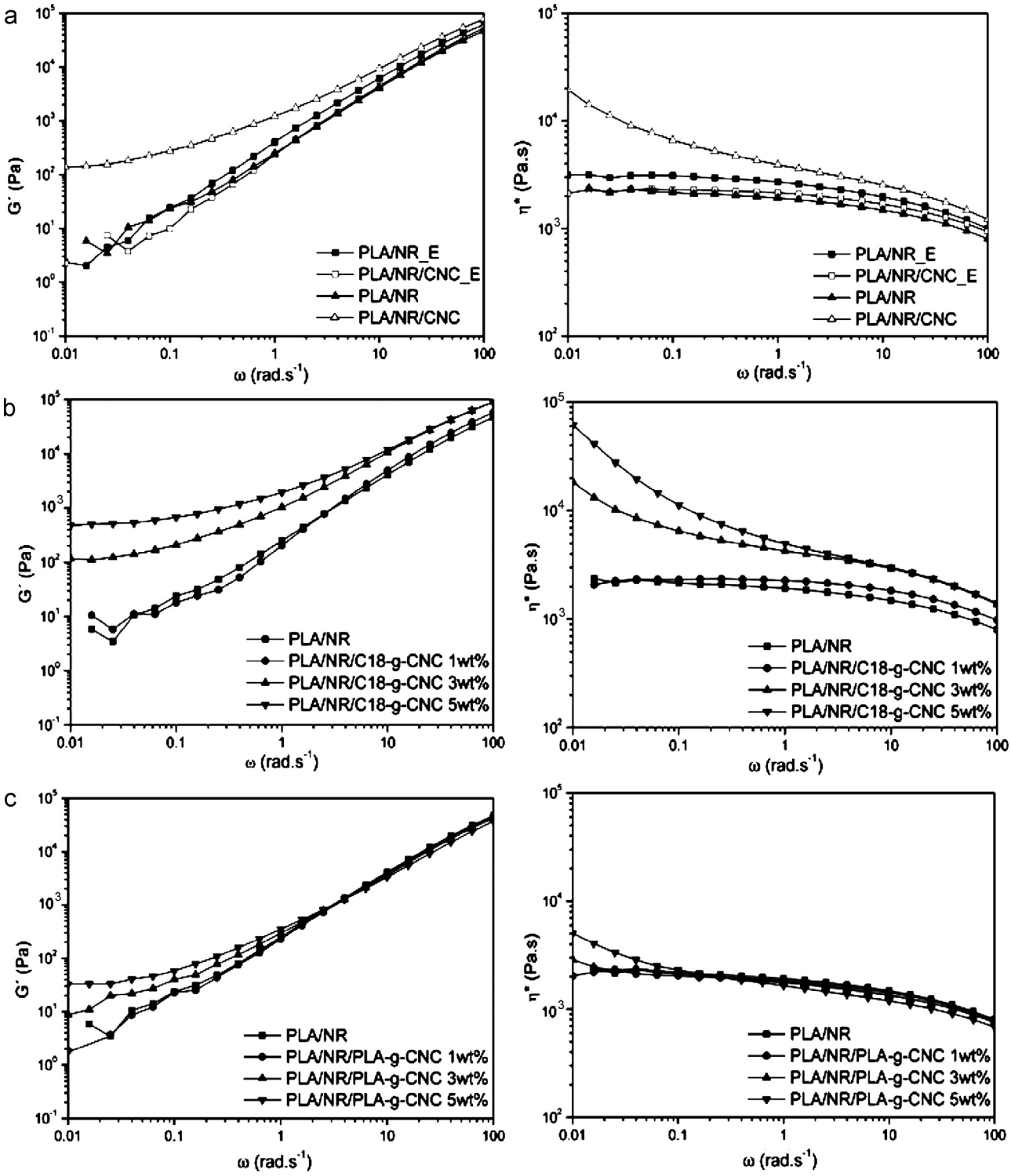

Fig. 6. (a) Influence of the blending procedure over the rheological properties of the materials and rheological properties of (b) PLA/NR/C18-g-CNC and (c) PLA/NR/PLA-g-CNC nanocomposites.

Also, the PLA-g-CNC are more agglomerated due to the presence of superficial PLA chains. Similar observations have been reported for PCL grafting (Habibi et al., 2008).

WAXD analysis of the nanocrystals was carried out in order to verify that the crystalline structure was maintained after the chemical modification (Fig. 5). Both CNC and C18-g-CNC display the typical diffraction peaks of cellulose I crystalline form (14.8°, 16.5°, 22.5° and 34.5°) (Bondeson et al., 2006). However, the diffraction peaks of C18-g-CNC are less sharp that the unmodified one, probably due to the formation of the grafted layer at the CNC surface and changes of the surface crystallinity.

The XRD pattern of the PLA-g-CNC displays two strong peaks located at $2\theta = 16.8°$ and 19.2° characteristics of the reflections of PLA crystalline α-form (Pan & Inoue, 2009). Moreover, weaker reflections are reported at 12.5°, 14.8°, 22.5° (Yasuniwa, Sakamo, Ono, & Kawahara, 2008). Thus, the CNC diffraction signal at 14.8°

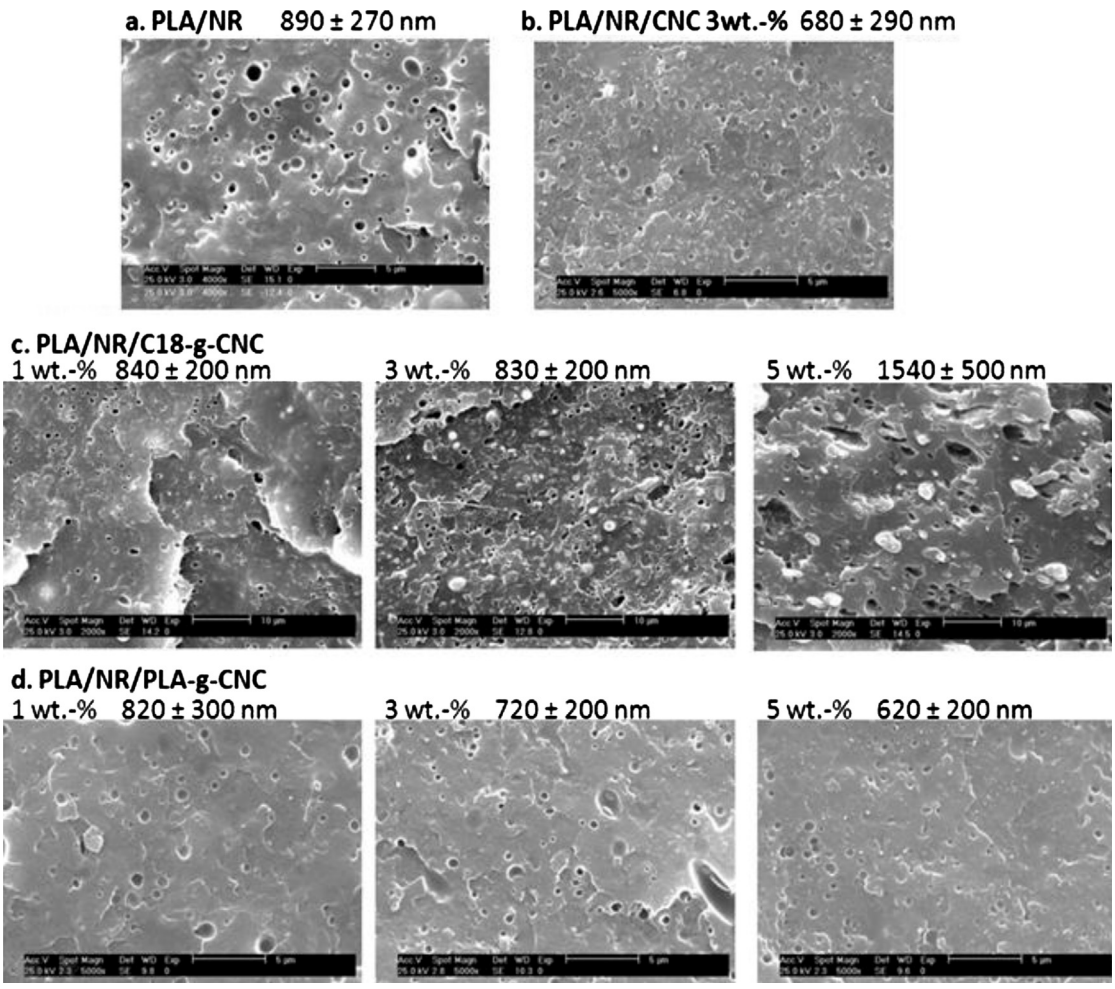

Fig. 7. SEM images of the materials and NR average droplets size of the materials.

and 16.5° are masked by the PLA crystalline diffraction. Cellulose and starch nanocrystals grafted with PCL by ring opening polymerization present similar behavior and no signal of nanoparticle crystals was detected due to PCL high crystallinity (Lin et al., 2009; Yu et al., 2008). However, in our case the unusual shape of the peak at 22.5° suggests that both CNC and PLA participate to the signal.

3.2. Optimization of processing

The preparation of bioparticle nanocomposites by extrusion often remains an issue due to the possible thermal degradation of cellulose whiskers. In this study, CNC were neutralized in order to prevent the degradation linked to the sulfate groups introduced during acid hydrolysis, and the same extrusion parameters as for the montmorillonite nanocomposites were applied, i.e. 180 °C, 100 rpm and 15 min (Bitinis et al., 2012b). However, strong degradation of cellulose nanowhiskers was observed when a PLA/NR/CNC blend was processed by direct extrusion at 180 °C and brown little spots could be seen in the material. Similar observation has been made by Goffin et al. (2011a). Thus, the processing temperature was reduced to 160 °C while time and rotor speed remained unchanged. No visible degradation was observed in this case.

Moreover, the crystalline structure of CNC could be prone to degradation during processing. Fig. 5b shows the XRD spectra for nanocomposites prepared by solvent casting combined with extrusion. Although the signal of crystalline CNC is very weak compared to the amorphous signal of the matrix, a shoulder is visible at 22.5°, corresponding to the most intense diffraction peak of cellulose I crystalline form. This signal is more visible for the nanocomposites at 5 wt.%. Therefore, it can be concluded that the crystalline structure of cellulose is maintained during processing, independently of the applied process conditions.

3.3. Rheological properties

The dispersion of CNC was also evaluated for PLA/NR/CNC 3 wt.% bionanocomposites prepared by both blending procedures. Rheology has been proven to be an effective tool to inform about the nanocomposite structure and measurements were carried out in frequency sweep mode (Cassagnau, 2008).

A slight difference of complex viscosity is observed between PLA/NR and PLA/NR_E at low frequencies in Fig. 6a. PLA chains are subjected to more aggressive conditions in the case of casting combined with extrusion, which explains the slight decrease of viscosity when compared to simple extrusion. Adding 3 wt.% of CNC does not lead to any changes in the case of direct extrusion, which suggests that nanoscale level dispersion is not achieved. Hence, agglomerates are expected to be present in the samples when redispersing dried CNC in the polymer matrix by direct extrusion. Interestingly, an increase of viscosity and storage modulus at low frequencies is observed when employing the solvent casting-extrusion method. This solid-like behavior is attributed to the formation of a network structure. Alloin, D'Aprea, Dufresne, El Kissi, and Bossard (2011) compared the rheological

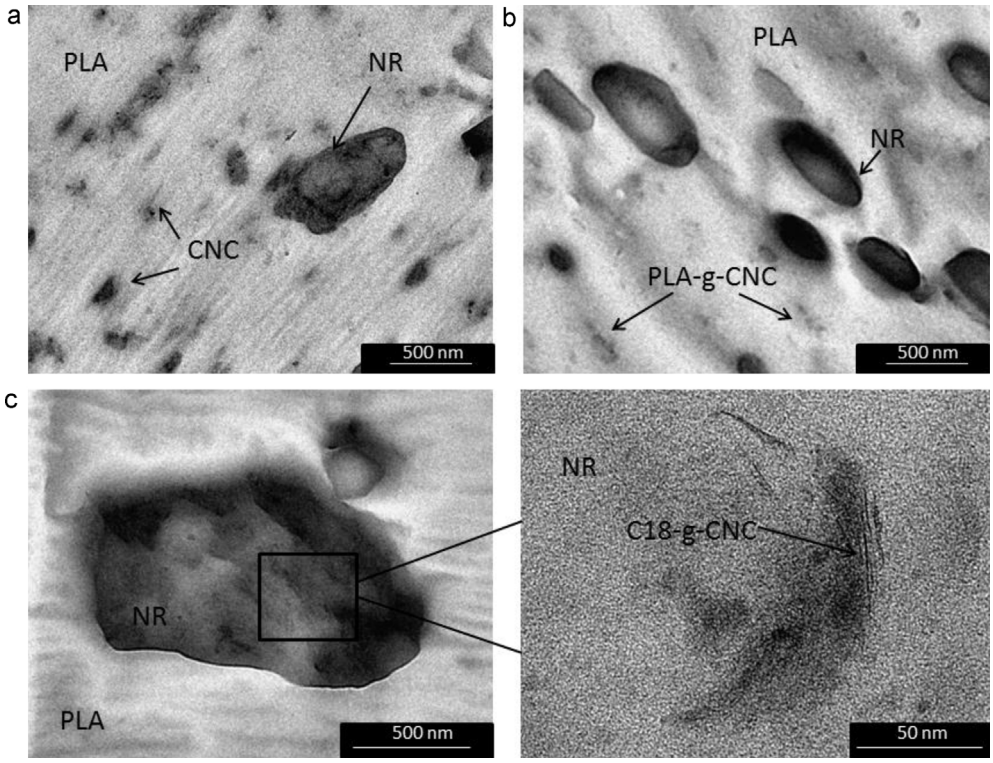

Fig. 8. TEM images of PLA/NR blend filled with (a) 3 wt.% CNC, (b) 5 wt.% PLA-g-CNC and (c) 5 wt.% C18-g-CNC at two magnifications.

properties of poly(oxyethylene)/ramie whiskers at 6 wt.% prepared by casting and by extruding a freeze-dried powder of the cellulose whiskers/POE solution. A solid-like behavior was reported for films prepared by casting while a liquid-like behavior was observed for films prepared by extrusion. They concluded that the extrusion prevented the formation of a strong whisker network.

Nevertheless, Fig. 6a shows that the network formation is preserved after extrusion and PLA/NR/CNC bionanocomposites having good dispersion of CNC can be successfully obtained using adequate process conditions. Thus, combining casting and extrusion has been the preferred processing method in this study. Jonoobi, Harun, Mathew, and Oksman (2010) developed a similar procedure and prepared a masterbatch of PLA/cellulose nanofibers by solvent casting before extrusion in order to improve the nanofiber dispersion.

Very few studies describe the rheological properties of cellulose nanowhisker composites (Alloin et al., 2011; Ben Mabrouk, Magnin, Belgacem, & Boufi, 2011; Goffin et al., 2011b). The authors reported solid-like behavior when strong interactions existed between the nanofiller and the matrix. As an example, Goffin et al. (2011b) studied PCL/CNC bionanocomposite viscoelastic properties, observing no effect of the pristine CNC while PCL-g-CNC induced a solid-like behavior at 8 wt.%. This behavior was due to the formation of a physical network between the polymer matrix and modified nanowhiskers.

The rheological properties of PLA/NR/C18-g-CNC bionanocomposites are reported in Fig. 6b. An increase of storage modulus G' and of the absolute complex viscosity η^* at low frequencies are observed for concentrations of 3 and 5 wt.% and a solid-like behavior is observed for 5 wt.%. Hence, the percolation threshold occurs between 3 and 5 wt.% loading fraction, confirming the formation of a network structure that gives to the material a better resistance against the applied deformation at low frequency. Fig. 6c shows the rheological properties of PLA/NR/PLA-g-CNC bionanocomposites. In this case, G' and η^* increase with the cellulose nanowhisker content, however this increment is lower and does not reach the solid-like behavior, probably due to the lower content of cellulose nanowhiskers in the modified CNC.

Nevertheless, the increase of the storage modulus and the complex viscosity are an indication that a good dispersion of the cellulose whiskers was achieved in both cases.

3.4. Morphology of the optimized bionanocomposites

Fig. 7 shows the morphology of PLA/NR blends filled with the three types of cellulose nanowhiskers. As already reported, PLA/NR blend presents a phase separated morphology with low interfacial adhesion between the two polymers (the microvoids of the SEM images are the result of the removal of the dispersed NR droplets during fracture) (Bitinis et al., 2012a, 2012b). A reduction of the size of NR domains is observed when compared to the unfilled blend when adding a 3 wt.% of unmodified CNC (Fig. 7b).

Further evolution of the morphology with the concentration of C18-g-CNC and PLA-g-CNC is reported in Fig. 7c and d. Increasing PLA-g-CNC concentration leads to a progressive reduction of the NR droplet size, while the opposite effect is reported for C18-g-CNC. The largest NR domains are observed for PLA/NR/C18-g-CNC 5 wt.%.

The affinity of the different types of CNC and their location in the blend need to be evaluated in order to explain these results. Given the polarity of the cellulose nanowhiskers, CNC affinity toward the PLA phase should be higher than that toward the NR domains. Moreover, in the case of the organoclay C15A, the presence of alkyl apolar chains in the clay lattices increased the affinity of the clay toward the NR domains (Bitinis et al., 2012b). The same effect is then expected for C18-g-CNC. Obviously, grafting PLA chains onto the CNC surface should improve its compatibility with the PLA matrix.

TEM images of PLA/NR blend filled with 3 wt.% of CNC, 5 wt.% of PLA-g-CNC and C18-g-CNC at 5 wt.% are shown in Fig. 8. TEM

contrast between polymers and cellulose nanowhiskers is low and complicates achieving TEM images with high resolution and high contrast. Nevertheless, CNC and PLA-g-CNC can be observed in the PLA matrix (Fig. 8a and b) even if it is not possible to observe single whiskers. In the case of C18-g-CNC, the PLA matrix appears to be very homogenous, confirming the absence of whiskers in this phase. C18-g-CNC is observed in the NR droplets, as seen in Fig. 8c and d. No whiskers could be seen at the interface between both polymers.

In general, the changes reported over the morphology of the blends can be ascribed to the changes of the viscosity ratio. The location of CNC and PLA-g-CNC in the PLA phase could increase the PLA viscosity and thus, hinder the coalescence of NR droplets facilitating the droplet break-up of the dispersed high viscosity rubber phase. The location of C18-g-CNC does not lead to important changes on the blend morphology at low filler loadings and a slight increase of NR droplets is observed for 5 wt.%. This effect could be ascribed to the increase of NR viscosity.

4. Conclusions

In this work, the extraction of nanocrystalline cellulose was performed from acid hydrolysis of commercial microcrystalline cellulose, obtaining rod-like crystals of 250 ± 80 nm in length. The grafting of both alkyl chains and PLA chains onto the cellulose nanowhiskers were successfully characterized achieving a grafting content of 20% and 70%, respectively. The efficiency of the grafting was more difficult to demonstrate for PLA-g-CNC. However, the high stability of PLA-g-CNC suspension in chloroform is a clear indication of the grafting success.

A special care was attributed to the processing method of new PLA/NR/CNC bionanocomposites, as a combination of casting and extrusion was necessary in order to prevent the degradation of the cellulose nanowhiskers and to obtain a good dispersion of the fillers. The addition of the three types of fillers affected the morphology of the blend, reducing the NR droplets in the case of PLA-g-CNC and CNC. These two nanowhiskers located in the PLA phase while C18-g-CNC was present in the rubbery phase. Nevertheless, no strong compatibilizing effect of the cellulose nanowhiskers was observed for the immiscible PLA/NR blend.

Further work will consist on the study of the resulting properties of the obtained bionanocomposites.

Acknowledgments

NB thanks the CSIC for a JAE-Pre grant. EF gratefully acknowledges the financial support from the National Consortium of Materials Science and Technology (INSTM).

References

Alloin, F., D'Aprea, A., Dufresne, A., El Kissi, N., & Bossard, F. (2011). Poly(oxyethylene) and ramie whiskers based nanocomposites: influence of processing: Extrusion and casting/evaporation. *Cellulose*, *18*(4), 957–973.

Angellier, H., Molina-Boisseau, S., Lebrun, L., & Dufresne, A. (2005). Processing and structural properties of waxy maize starch nanocrystals reinforced natural rubber. *Macromolecules*, *38*(9), 3783–3792.

Azizi Samir, M. A. S., Alloin, F., & Dufresne, A. (2005). Review of recent research into cellulosic whiskers, their properties and their application in nanocomposite field. *Biomacromolecules*, *6*(2), 612–626.

Beck-Candanedo, S., Roman, M., & Gray, D. G. (2005). Effect of reaction conditions on the properties and behavior of wood cellulose nanocrystal suspensions. *Biomacromolecules*, *6*(2), 1048–1054.

Ben Mabrouk, A., Magnin, A., Belgacem, M. N., & Boufi, S. (2011). Melt rheology of nanocomposites based on acrylic copolymer and cellulose whiskers. *Composites Science and Technology*, *71*(6), 818–827.

Bitinis, N., Sanz, A., Nogales, A., Verdejo, R., Lopez-Manchado, M. A., & Ezquerra, T. A. (2012). Deformation mechanisms in polylactic acid/natural rubber/organoclay bionanocomposites as revealed by synchrotron X-ray scattering. *Soft Matter*, *8*(34), 8990–8997.

Bitinis, N., Verdejo, R., Maya, E. M., Espuche, E., Cassagnau, P., & Lopez-Manchado, M. A. (2012). Physicochemical properties of organoclay filled polylactic acid/natural rubber blend bionanocomposites. *Composites Science and Technology*, *72*(2), 305–313.

Bondeson, D., Mathew, A., & Oksman, K. (2006). Optimization of the isolation of nanocrystals from microcrystalline cellulose by acid hydrolysis. *Cellulose*, *13*(2), 171–180.

Bondeson, D., & Oksman, K. (2007). Dispersion and characteristics of surfactant modified cellulose whiskers nanocomposites. *Composite Interfaces*, *14*(7–9), 617–630.

Bordes, P., Pollet, E., & Averous, L. (2009). Nano-biocomposites: Biodegradable polyester/nanoclay systems. *Progress in Polymer Science*, *34*(2), 125–155.

Cassagnau, P. (2008). Melt rheology of organoclay and fumed silica nanocomposites. *Polymer*, *49*(9), 2183–2196.

Darder, M., Aranda, P., & Ruiz-Hitzky, E. (2007). Bionanocomposites: A new concept of ecological, bioinspired, and functional hybrid materials. *Advanced Materials*, *19*(10), 1309–1319.

Favier, V., Canova, G. R., Cavaille, J. Y., Chanzy, H., Dufresne, A., & Gauthier, C. (1995). Nanocomposite materials from latex and cellulose whiskers. *Polymers for Advanced Technologies*, *6*(5), 351–355.

Fenouillot, F., Cassagnau, P., & Majeste, J. C. (2009). Uneven distribution of nanoparticles in immiscible fluids: Morphology development in polymer blends. *Polymer*, *50*(6), 1333–1350.

Fortunati, E., Armentano, I., Zhou, Q., Iannoni, A., Saino, E., Visai, L., et al. (2012). Multifunctional bionanocomposite films of poly(lactic acid), cellulose nanocrystals and silver nanoparticles. *Carbohydrate Polymers*, *87*(2), 1596–1605.

Fortunati, E., Peltzer, M., Armentano, I., Torre, L., Jimenez, A., & Kenny, J. M. (2012). Effects of modified cellulose nanocrystals on the barrier and migration properties of PLA nano-biocomposites. *Carbohydrate Polymers*, *90*(2), 948–956.

Franklin, W. E. (1979). Direct pyrolysis of cellulose and cellulose derivatives in a mass spectrometer with a data system. *Analytical Chemistry*, *51*(7), 992–996.

Goffin, A.-L., Raquez, J.-M., Duquesne, E., Siqueira, G., Habibi, Y., Dufresne, A., et al. (2011). From interfacial ring-opening polymerization to melt processing of cellulose nanowhisker-filled polylactide-based nanocomposites. *Biomacromolecules*, *12*(7), 2456–2465.

Goffin, A. L., Raquez, J. M., Duquesne, E., Siqueira, G., Habibi, Y., Dufresne, A., et al. (2011). Poly(epsilon-caprolactone) based nanocomposites reinforced by surface-grafted cellulose nanowhiskers via extrusion processing: Morphology, rheology, and thermo-mechanical properties. *Polymer*, *52*(7), 1532–1538.

Habibi, Y., Goffin, A.-L., Schiltz, N., Duquesne, E., Dubois, P., & Dufresne, A. (2008). Bionanocomposites based on poly(epsilon-caprolactone)-grafted cellulose nanocrystals by ring-opening polymerization. *Journal of Materials Chemistry*, *18*(41), 5002–5010.

Habibi, Y., Lucia, L. A., & Rojas, O. J. (2010). Cellulose nanocrystals: chemistry, self-assembly, and applications. *Chemical Reviews*, *110*(6), 3479–3500.

Henriksson, M., Berglund, L. A., Isaksson, P., Lindstrom, T., & Nishino, T. (2008). Cellulose nanopaper structures of high toughness. *Biomacromolecules*, *9*(6), 1579–1585.

Jonoobi, M., Harun, J., Mathew, A. P., & Oksman, K. (2010). Mechanical properties of cellulose nanofiber (CNF) reinforced polylactic acid (PLA) prepared by twin screw extrusion. *Composites Science and Technology*, *70*(12), 1742–1747.

Julien, S., Chornet, E., & Overend, R. P. (1993). Influence of acid pretreatment (H_2SO_4, HCl, HNO_3) on reaction selectivity in the vacuum pyrolysis of cellulose. *Journal of Analytical and Applied Pyrolysis*, *27*(1), 25–43.

Kim, D. Y., Nishiyama, Y., Wada, M., & Kuga, S. (2001). High-yield carbonization of cellulose by sulfuric acid impregnation. *Cellulose*, *8*(1), 29–33.

Le Corre, D., Bras, J., & Dufresne, A. (2010). Starch nanoparticles: A review. *Biomacromolecules*, *11*(5), 1139–1153.

Lin, N., Chen, G., Huang, J., Dufresne, A., & Chang, P. R. (2009). Effects of polymer-grafted natural nanocrystals on the structure and mechanical properties of poly(lactic acid): A case of cellulose whisker-graft-polycaprolactone. *Journal of Applied Polymer Science*, *113*(5), 3417–3425.

Pan, P., & Inoue, Y. (2009). Polymorphism and isomorphism in biodegradable polyesters. *Progress in Polymer Science*, *34*(7), 605–640.

Pappa, A., Mikedi, K., Tzamtzis, N., & Statheropoulos, M. (2003). Chemometric methods for studying the effects of chemicals on cellulose pyrolysis by thermogravimetry-mass spectrometry. *Journal of Analytical and Applied Pyrolysis*, *67*(2), 221–235.

Pappa, A., Mikedi, K., Tzamtzis, N., & Statheropoulos, M. (2006). TG-MS analysis for studying the effects of fire retardants on the pyrolysis of pine-needles and their components. *Journal of Thermal Analysis and Calorimetry*, *84*(3), 655–661.

Pappa, A. A., Tzamtzis, N. E., Statheropoulos, M. K., Liodakis, S. E., & Parissakis, G. K. (1995). A comparative study of the effects of fire retardants on the pyrolysis of cellulose and pinus-helepensis pine-needles. *Journal of Analytical and Applied Pyrolysis*, *31*, 85–100.

Pei, A. H., Zhou, Q., & Berglund, L. A. (2010). Functionalized cellulose nanocrystals as biobased nucleation agents in poly(L-lactide) (PLLA) – Crystallization and mechanical property effects. *Composites Science and Technology*, *70*(5), 815–821.

Petersson, L., Kvien, I., & Oksman, K. (2007). Structure and thermal properties of poly(lactic acid)/cellulose whiskers nanocomposite materials. *Composites Science and Technology*, *67*(11–12), 2535–2544.

Rhim, J. W. (2007). Potential use of biopolymer-based nanocomposite films in food packaging applications. *Food Science and Biotechnology*, *16*(5), 691–709.

Roman, M., & Winter, W. T. (2004). Effect of sulfate groups from sulfuric acid hydrolysis on the thermal degradation behavior of bacterial cellulose. *Biomacromolecules*, *5*(5), 1671–1677.

Siqueira, G., Bras, J., & Dufresne, A. (2010). New process of chemical grafting of cellulose nanoparticles with a long chain isocyanate. *Langmuir*, *26*(1), 402–411.
Statheropoulos, M., & Kyriakou, S. A. (2000). Quantitative thermogravimetric-mass spectrometric analysis for monitoring the effects of fire retardants on cellulose pyrolysis. *Analytica Chimica Acta*, *409*(1–2), 203–214.
Uschanov, P., Johansson, L.-S., Maunu, S. L., & Laine, J. (2011). Heterogeneous modification of various celluloses with fatty acids. *Cellulose*, *18*(2), 393–404.
Wang, N., Ding, E., & Cheng, R. (2007). Thermal degradation behaviors of spherical cellulose nanocrystals with sulfate groups. *Polymer*, *48*(12), 3486–3493.
Yasuniwa, M., Sakamo, K., Ono, Y., & Kawahara, W. (2008). Melting behavior of poly(L-lactic acid): X-ray and DSC analyses of the melting process. *Polymer*, *49*(7), 1943–1951.
Yu, J. H., Ai, F. J., Dufresne, A., Gao, S. J., Huang, J., & Chang, P. R. (2008). Structure and mechanical properties of poly(lactic acid) filled with (starch nanocrystal)-graft-poly(epsilon-caprolactone). *Macromolecular Materials and Engineering*, *293*(9), 763–770.